CrystEngComm

Accepted Manuscript

ROYAL SOCIETY OF CHEMISTRY

www.rsc.org/crystengcomm

CrystEngComm

RSCPublishing

ARTICLE

Silk Fibroin-Mediated Biominerlization of Calcium Carbonate at the Air/Water Interface

Cite this: DOI: 10.1039/x0xx00000x

Wei Hao,[a] David Porter,[b] Xianting Wang[a] and Zhengzhong Shao*[a]

Received 00th January 2012,
Accepted 00th January 2012

DOI: 10.1039/x0xx00000x

www.rsc.org/

The synthesis of calcium carbonate ($CaCO_3$) with different morphologies and polymorphs at the air/water interface has been reported in previous work, while the influence of the structure of macromolecular additives on this type of mineralization is rarely investigated. Regenerated silk fibroin (RSF) from the *Bombyx mori* silkworm silk is analogous to the main protein contained in naturally formed nacre, which can form complex structures at the air/water interface due to the multi-block amphipathy. This study demonstrates how a range of $CaCO_3$ structures with a variety of different morphologies and polymorphs were obtained at the air/water interface mediated by RSF. The precursor stabilizing ability of RSF allows the crystals to grow directly from amorphous calcium carbonate (ACC), which is observed by time-dependent experiments. The structures of RSF that exist at the interface determine the final morphologies and polymorphs of the crystals, which can be influenced by the concentrations of ([RSF] and [Ca^{2+}]) and the molecular weight of RSF. Thermodynamically metastable aragonite phase may be mediated by β-sheets of RSF formed at low concentrations, while stable calcite can be generated by the RSF amorphous structure at high concentrations. The synergy between RSF and $CaCO_3$ at the interface can provide a way to understand the function of organic materials involved in the biomineralization process, and can be applied to manipulate the structures of synthetic hybrid materials.

Introduction

Calcium carbonate ($CaCO_3$) is one of the most abundant minerals in nature, used as a structural or protective material. The preparation of highly regulated $CaCO_3$ with fine structures under ambient conditions has attracted much attention.[1, 2] During the biomineralization process, both the water-soluble fraction and the insoluble matrix of organic materials are considered to play essential roles.[3] For example, the soluble acid glycoproteins combining with silk fibroin-like proteins with regular β-sheet structure have a strong influence on the morphology and lattice structure of minerals, while insoluble β-chitin serves as a nucleation surface and template in mollusk shell nacre.[4] Therefore, to mimic the biomineralization phenomena of natural organisms *in vitro*, the design and preparation of organic matrices (soluble and insoluble) is an active and fertile area of research. Insoluble templates such as rigid solid matrices (fibre, membrane, scaffold),[5] self-assembled monolayers,[6] and Langmuir-Blodgett (LB) films at the air/water interface[1, 7-9] can all guide inorganic crystal morphology into remarkable forms.

Amphiphilic molecules can self-assemble at an air/water interface, whose conformation is different from that in the bulk solution. Thus they can be used to produce asymmetric inorganic particles or films,[7, 8, 10, 11] and the chain length can affect crystallization.[11] Particularly, various proteins can form more complex films at the air/water interface due to the high molecular weight and/or muti-block hydrophilic/hydrophobic segments. The structure and morphology of the protein self-assembled film depend on many factors; for example, concentration of the bulk solution, temperature and molecular weight.[12, 13] However, much previous work has focused on the solution-phase mineralization mediated by proteins, while the influence of the self-assembled film structures on templated crystallization at the interface still need to be studied.

Regenerated *Bombyx mori* silk fibroin (RSF) is similar to silk fibroin-like proteins in nacre, both in the amino acid composition and secondary structure.[14] Work in our laboratory has shown that RSF dominated by β-sheet conformation in solution presents a strong preference for the formation of the aragonite phase of $CaCO_3$.[15] RSF is a hydrophilic/hydrophobic partitioning molecule, which can separate its hydrophilic and hydrophobic residues on opposite sides of the interface when it adsorbed at an air/water interface.[16, 17] Yang *et al* have studied the behaviour of RSF at the air/water interface and found that the dynamic surface tension and structure of RSF are dependent on the solution concentration.[12] In this paper, we focus on the effect of concentration of ([RSF] and [Ca^{2+}]), and RSF molecular weight on $CaCO_3$ templating in an ammonium carbonate diffusion system. A continuous change in the polymorphs and morphology of the final $CaCO_3$ products could be linked with the structure of RSF adsorbed layers at the air/water interface. Time-dependent observations are used to reveal the crystallization process mediated by RSF. Based on these results, we

suggest a possible mechanism for the mineralization at the air/water interface.

Experimental Section

Materials and Preparation of Regenerated Silk Fibroin Solution. RSF aqueous solutions were prepared from natural *Bombyx mori* silkworm cocoons. To obtain RSF with varied molecular weights, we used different degumming methods following established procedures.[18] The silk cocoons were first treated with 0.5 wt% Na_2CO_3 or $NaHCO_3$ boiling solution to remove sericin and the degummed silk then dissolved in 9.5 mol/L LiBr aqueous solution. After being filtered, the RSF/inorganic solvents were dialyzed against deionized water for 72 h to remove inorganic ions. The dialyzed solutions were then clarified by spinning in a centrifuge at 6000 rpm for about 8 min. The supernatant with about 4 wt% (w/w) of RSF was collected and stored at 4 °C. Different concentration solutions were prepared at room temperature. The molecular weights were tested by rheological measurements, described in detail elsewhere.[19] The labels and preparation processes of different RSF solutions are summarized in Table 1.

Table 1 Labels and preparation of different RSF solutions

Label	M_w (kDa)	M_w/M_n	Degumming process	Dissolving reagent
RSF-185	185	1.05	$NaHCO_3$ for 60 min	LiBr
RSF-83	83	1.95	Na_2CO_3 for 45 min	LiBr
RSF-36	36	1.58	Na_2CO_3 for 180 min	LiBr

Crystallization of $CaCO_3$. In preparation, the glass substrates and beakers were subjected to ultrasound in ethanol and deionized water (DIW) for 30 min, further soaked in H_2O-HNO_3(65 wt%)-H_2O_2(1:1:1, v/v/v) solution, then rinsed with DIW and finally dried in an oven at 80 °C. Mineralization was carried out in a 10 mL beaker containing a mixture solution of an appropriate amount of RSF (RSF-83 was employed if no further noted) solution in the range of 0.0001 wt% to 2 wt% and $CaCl_2$ solution in the range of 1 mM to 10 mM. The beaker was covered by parafilm with six pinholes and then transferred into a large closed desiccator (about 6.5 L). 3 g of freshly crushed ammonium carbonate was put in another 10 mL beaker covered with parafilm with 6 pinholes, and placed into the desiccator for releasing CO_2. The mineralization temperature was around 25 °C. After an assigned time, a glass substrate or copper grid was used to carefully collect the $CaCO_3$ particles produced at the air/water interface. The obtained $CaCO_3$ particles were dried in air for further characterization. For Laser Confocal Fluorescence Micrograph characterization, the particles were washed by DIW and obtained by centrifuging. This process was repeated 3 times and the sediments were dried in air before observation.

Characterization. The morphologies of the $CaCO_3$ particles were observed with a TS 5136MM scanning electron microscope (SEM) at 20 KV after sputtered with gold (about 5 nm to 20 nm of the thickness). High-magnification images were obtained on an S-4800 FE-SEM at 1 KV. Transmission electron microscopy (TEM), high-resolution transmission electron microscopy (HRTEM) images, selective area electron diffraction (SAED) patterns and Electron diffraction (EDX) were obtained on a JEM-2100F operated at 200 KV. The polymorphs of $CaCO_3$ were detected on a Renishaw inVia Reflex Raman spectrometer equipped with a Leica 2500 optical microscope and 633 nm Helium/Neon laser, CCD detector. Visual observations were performed by polarized optical microscopy (Olympus BX61). Fluorescence observations were performed by Laser confocal fluorescence microscopy (Olympus FV 1000), the excitation wavelength was 405 nm.

Results and Discussion

RSF is recognized as a multi-block amphiphilic macromolecule, thus can adsorb on the surface and change the surface tension.[20] Yang *et al.*[13] used a video-enhanced drop shape tensiometry technique to characterize the surface activity, and found the equilibrium surface tension of RSF solutions was constant above a bulk concentration of 2 wt%, and ascribed this to the formation of aggregates in the bulk solution. In the diluted RSF solution (≤ 2 wt%), the adsorption mechanisms and structure of RSF were depending on the bulk concentration. With our system, we measured the RSF solution surface tension in different concentrations of $CaCl_2$ (1 mM, 5 mM and 10 mM) using the Wilhelmy plate method (Supporting Information, Figure S1). It was found that increasing the concentration of RSF from 0.0002 wt% to 2 wt% in the bulk solution can decrease the surface tension at all concentrations of $CaCl_2$, and the decline of surface tension is slowed down at higher concentrations of RSF, which may be ascribed to the formation of aggregates in the bulk solution. This trend is in accordance with Yang's research, and may affect the mineralization process. Therefore, RSF solutions with concentration less than 2% were selected for the mineralization of $CaCO_3$ as the additive.

In the controlled mineralization without any additive, the $CaCO_3$ particles produced at the air/water interface were conventional rhombohedral calcite with little vaterite (Figure S2). The addition of RSF to the mineralization solution greatly changed the polymorph and morphology of the $CaCO_3$ particles. Figure 1 shows how the morphologies of $CaCO_3$ particles varied with the concentration of RSF and Ca^{2+}. The polymorphs of the particles were detected by Raman (Figure S3) and summarized in Table 2.

The two main crystal polymorphs obtained at the air/water interface are calcite and aragonite. In general, large calcite crystals could be obtained with relatively high bulk concentrations of RSF and Ca^{2+} (shown in the darker grey areas in Table 2), while aragonite particles became the domain polymorph under conditions of low bulk component concentrations (displayed with lighter grey in Table 2). The domain crystal polymorphs showed a gradual transition from calcite to aragonite with decreased [RSF] at a fixed Ca^{2+} concentration. The coexisting point of two polymorphs shifted to lower RSF concentration with increasing Ca^{2+} concentration.

With reducing RSF concentration, the morphology of the calcite particles changed from flower-like structures (Figure 2a, 2b) to rhombohedral with a stepped indentation upper surface and rounded corners (Figure 2c, 2d). When the RSF concentration was extremely low, Ca^{2+} cannot reach the critical nucleation point on the RSF chains, which resulted in conventional rhombohedral calcite similar to the control experiment, due to thermodynamic stability (Figure 2e, 2f). Classical crystallization might be dominant in control experiments and those of low concentrations of RSF.

The continuous morphology and polymorph variation can also be observed in the aragonite crystals obtained with decreasing RSF concentration when $[Ca^{2+}]$ = 1 mM. The two ends of bundle-like aragonite, namely the fan-shape sectors, become gradually wider, and the final size becomes larger. When further decreasing the RSF concentration, the low content of RSF at the air/water interface causes the irregular bundle-like aragonite. When increasing Ca^{2+} concentration to 5 mM and 10 mM, both the size and quantity of these calcite particles increased at high RSF concentration, and the fan-shape sectors of the aragonite become wider. Besides the bundle-like aragonite morphology, large hemisphere aragonite particles were produced at high component concentration, which were printed in bold and italic type "***A***" in Table 2. The size of hemisphere

aragonite obtained under calcite domain condition is much smaller than under other conditions.

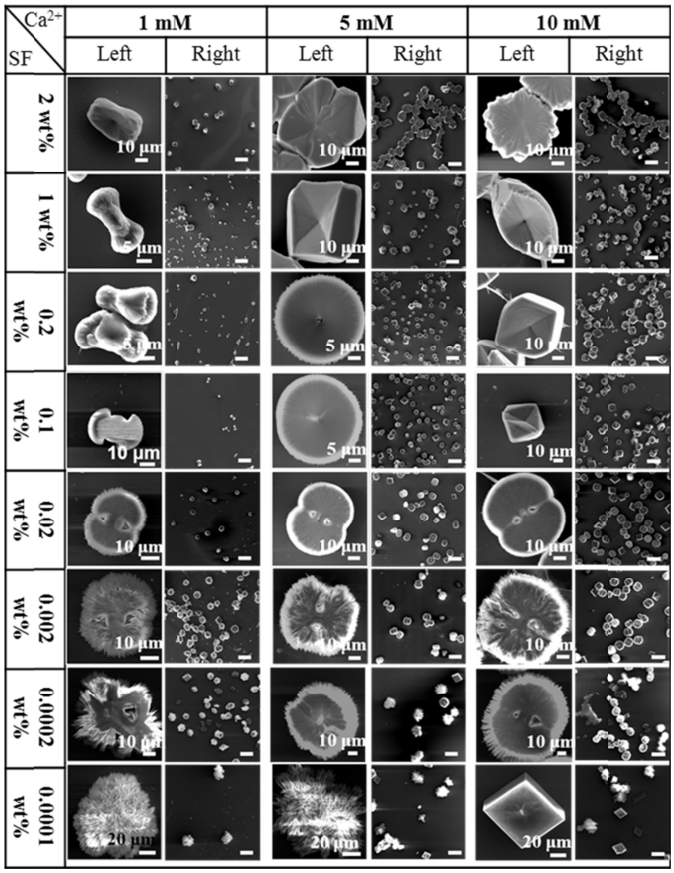

Figure 1 SEM images of $CaCO_3$ crystals collected at the air/water interface with different concentrations of RSF-83 and Ca^{2+} (as noted in the figure). The microscope images are upper surface views. Left images are the enlarge images of the dominate crystal in right images. Mineralization time: 72 h. Bars in right images are 100 μm.

Table 2 $CaCO_3$ polymorphs obtained at the air/water interface with different concentrations of RSF-83 and Ca^{2+}

RSF / Ca^{2+}	2 wt%	1 wt%	0.2 wt%	0.1 wt%	0.02 wt%	0.002 wt%	0.0002 wt%	0.0001 wt%
1 mM	C	A+C	A+C	A	A	A	A+V/***C***	A+***C***/V
5 mM	C	C+***A***	***A***+C	***A***	A	A	A+***C***	A+***C***
10 mM	C	C+***A***	C+***A***	C+***A***	A+C	A+***C***	A+***C***	A+***C***

Note: The capitals— C, A and V, are the abbreviations for calcite, aragonite and vaterite, respectively. "A+C" suggests that aragonite and calcite coexisted at the interface, while aragonite was the dominate crystal. "V/C" indicates that the number of vaterite and calcite particles were much the same. "***A***" printed in bold and italic type represents hemisphere aragonite, while "A" indicates bundle-like aragonite. "***C***" printed in bold and italic type represents the conventional rhombohedral calcite obtained at low RSF concentration. The data were summarized from Raman and SEM images. Different dominant crystal polymorphs are represented with different color boxes.

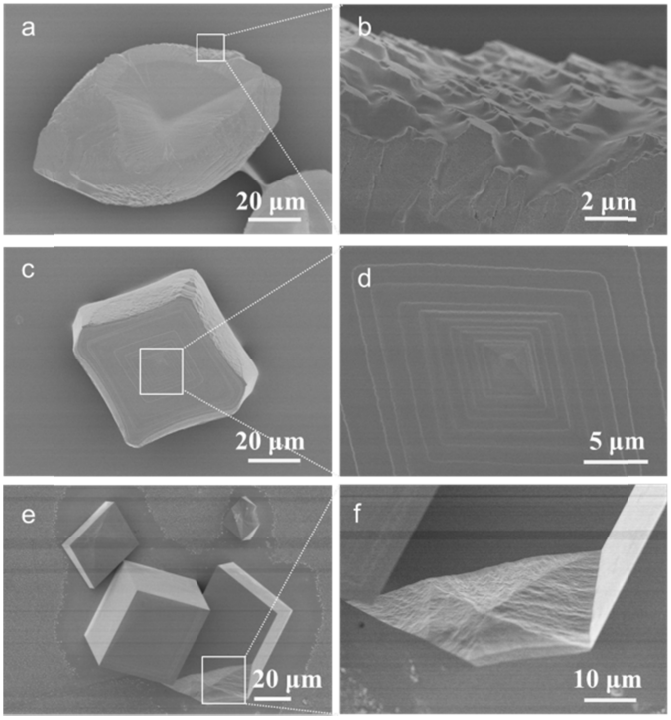

Figure 2 FE-SEM images of the calcite particles obtained at the air/water interface under different component concentrations. (a) and (b) [RSF-83] = 1 wt%, $[Ca^{2+}]$ = 10 mM; (c) and (d) [RSF-83] = 0.2 wt%, $[Ca^{2+}]$ = 10 mM; (e) and (f) [RSF-83] = 0.0001 wt%, $[Ca^{2+}]$ = 10 mM.

To gain insight into the formation process of the aragonite products, we looked in detail at the development of crystal morphology under two selected sets of condition. First, with the conditions of ([RSF] = 0.1 wt%, $[Ca^{2+}]$ = 5 mM), the growth process of hemisphere aragonite is shown in Figure 3. After mineralization for 2 h, nothing can be observed by the unaided eye, but some relatively dark particles can be seen in the TEM image (Figure 3a). Selective area electronic diffraction (SAED) pattern of the corresponding area indicates that the particles were aragonite (inset in Figure 3a). These particles are also present in the SEM image (Figure 3b), but their structure can be destroyed under low-energy (1 KV) electron irradiation (inset in Figure 3b), which suggests the partially amorphous nature of these particles. With the reaction time increased to 4 h, some hemi-gourd aragonite particles with an indentation in the middle of the upper surface are detected (Figure 3c). When the mineralization is extended, the aragonite particles become larger. We can see from the back-view after 6 h (Figure 3d) and side-view after 8 h (Figure 3e) of the hemisphere aragonite that the crystals are composed of nanoneedles, which are similar to the units of aragonite obtained in the bulk solution at high component concentration.[15] The size of the aragonite further increases after crystallization for 10 h (Figure 3f). Some nanowires connecting two particles (Figure 3g) and a few irregular calcite particles (Figure 3h) can be observed in the last stage of mineralization. We can see the nanowires located between two hemisphere crystals (Figure 3i, 3j), but they are not on the same height level with the crystal's upper surface (Figure 3g) and some of them are broken (Figure 3g). These nanowires are speculated to be dry state of the mother liquors between two particles after they are collected from air/water interface. Besides the nanowires, irregular material can also be found adhered to the nanoneedles at the edge of the hemisphere when mineralization is extended to 72 h (Figure 3k).

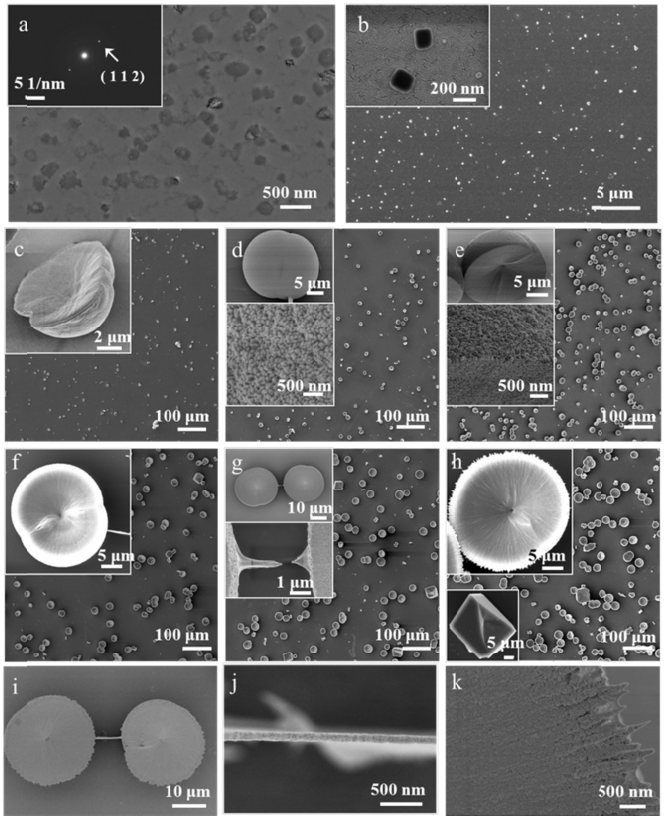

Figure 3 TEM (a) and SEM (b-k) images of $CaCO_3$ collected at the air/water interface at different mineralization times. [RSF-83] = 0.1 wt%, $[Ca^{2+}]$ = 5 mM. (a) and (b) 2 h; (c) 4 h; (d) 6 h; (e) 8 h; (f) 10 h; (g) 24 h and (h-k) 72 h. Inset in (a) indicates SAED pattern of $CaCO_3$. The spots show that the d-spacing values corresponding to aragonite (112). The parameters of the crystal are referenced to (76-0606). Insets in (b-g) show the detailed aragonite images. The top left corner inset of (h) indicates aragonite particle and the lower left corner inset of (h) represents calcite particle. (j) and (k) are the magnified images of (i).

For the second set of conditions, when [RSF] = 0.02 wt%, $[Ca^{2+}]$ = 1 mM, bundle-like aragonite particles can be produced at the air/water interface (Figure 4). The SEM image of the sample obtained at 2 h is shown in Figure 4a, from which some unstable nanoparticles are observed. After mineralizing for 4 h, some "shuttle-like" structure on which new spikes evolved at one end and an indentation in the upper surface can be seen. In a subsequent step, the structure starts to branch with an expansion in size over the following hours, and finally form a well-defined bundle-like aragonite (Figure 4c-4f). We can see from the front view (Figure 4g) and back view (Figure 4h) of the bundle-like aragonite collected at 72 h that the crystals consisted of nano-needles, which are bigger in size than the units in hemisphere particles (Figure 3d, 3e). These units are similar to that of aragonite collected in the bulk solution with low component concentration.[15] An obvious boundary can be seen on the upper surface of bundle-like aragonite (lower left corner inset of Figure 4g), which is highlighted by the dotted white line (top right corner inset of Figure 4g). The structure of the depressed section in the middle is looser than the remaining part. Moreover, the nanoneedles are smoother on the backside than those on the upper surface (Figure 4h).

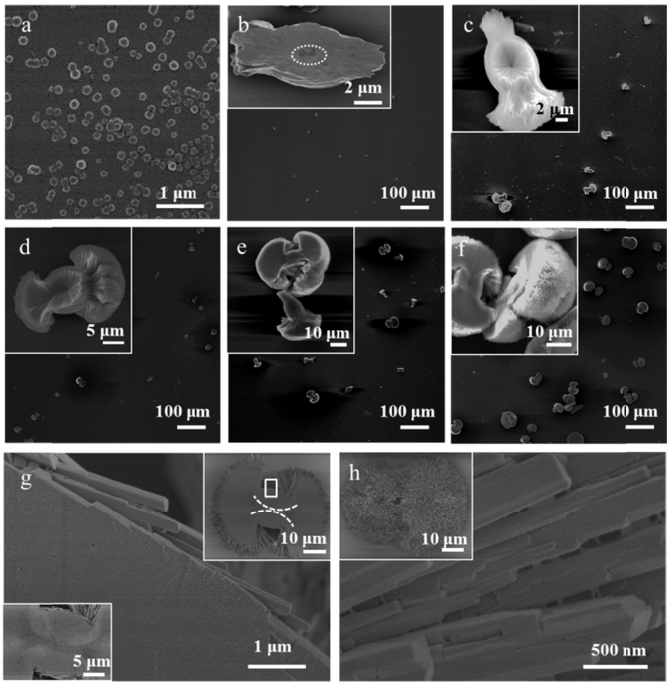

Figure 4 SEM images of $CaCO_3$ collected at the air/water interface at different mineralization times. [RSF-83] = 0.02 wt%, $[Ca^{2+}]$ = 1 mM. (a) 2 h; (b) 4 h; (c) 6 h; (d) 8 h; (e) 10 h; (f) 24 h; (g) and (h) 72 h. The dotted lines in insets of (b) and (g) outline the feature of particle inner shape. The top right corner inset of (g) indicates the whole aragonite particle, and the lower left corner inset of (g) shows the inner detail image. (g) indicates the side detail image of aragonite particle highlighted in the solid square. (h) is the back side of the aragonite particle.

The growth process of the aragonite particles is very similar to polymer spherulites, which consist of radial growth fibers, and with strong birefringence. Clear Maltese Crosses can be observed from the hemisphere aragonite particles obtained in our experiments, which can further verify the similarity between the aragonite and polymer spherulites (Figure 5).

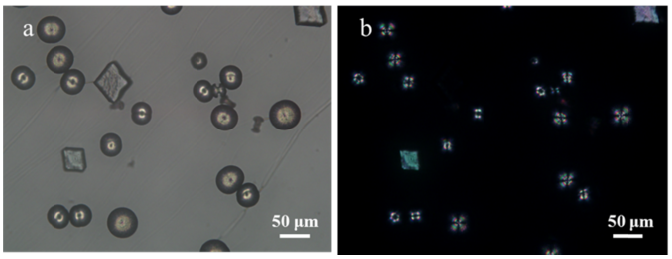

Figure 5 Light and polarized optical microscope images of images of aragonite particles obtained at the air/water interface with [RSF-83] = 0.1 wt%, $[Ca^{2+}]$ = 5 mM. Mineralization time: 72 h.

TEM was applied to further investigate the structure of the hemisphere aragonite particles. Nanoneedles at the edge of the crystals mineralized for 24 h show a well-defined characteristic of crystals viewed along the [010] direction, and the long axis of the needle is [001] (Figure 6a, 6b). This crystal lattice structure is in accord with the aragonite produced in the bulk solution.[15] RSF has proven extremely versatile in its control over the nucleation and growth of aragonite because of the excellent match in the ionic spacing in the β-strand conformers and the aragonite (010) plane.[15] TEM shows that the upper surface of the particle parallel to the

air/water interface is aragonite (010) plane. We suppose here the ionic spacing of β-structure (β-strand or β-sheet) is the same in the RSF chains existing in both the bulk solution and the air/water surface layer (or subsurface layer). Then it could be speculated that β-sheets (or β-strands) in RSF chain at the interface could be absorbed onto the aragonite crystal (010) face, by electrostatic interactions between the negatively charged oxygen atom in the C=O group and positively charged Ca^{2+}, resulting in the aragonite crystal growing along the [001] long axis.

In the TEM image of the crystal mineralized for 72 h, we can see some irregular material near the nanoneedles that shows relatively low contrast (Figure 6c). No crystal lattice can be observed in the HRTEM image of the irregular material (Figure 6d), also not in the nanowires connecting two particles, which was already found in SEM (Figure 6e, 6f). SAED of the nanowires shows a dispersion ring. Element analysis indicates that they are mainly composed of Ca, O and C (Figure 6f). Therefore, the material near the nanoneedles and nanowires connecting two particles are speculated to be amorphous calcium carbonate (ACC).

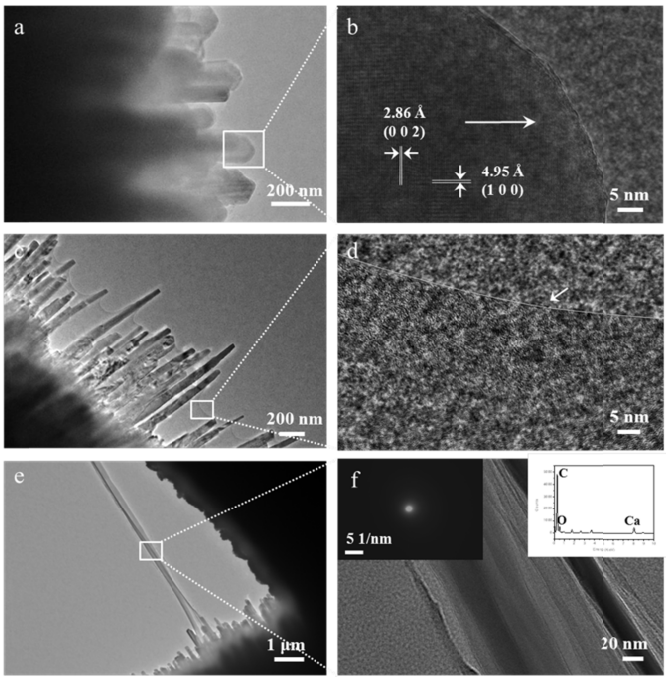

Figure 6 TEM images of $CaCO_3$ collected at the air/water interface. [RSF-83] = 0.1 wt%, [Ca^{2+}] = 5 mM. (a) (b) represent nanoneedles on the edge of particles which were mineralized for 24 h. HRTEM images in (b) represents orientation along the [010] zone axis. The arrow shows [001] direction along the long axis of the crystals. (c) shows the edge of particles mineralized for 72 h. (d) shows the irregular material between the nanoneedles. The arrow in (d) points out the boundary between the irregular material and the blank area. (e) represents the nanowire between two $CaCO_3$ particles. (f) is the enlarged image of the nanowire. The ED pattern and EDX spectrum indicates the line is comprised of ACC.

To further unravel the interaction between RSF and the crystals, we observed the particles obtained at the air/water interface under fluorescence microscopy. Our lab has found that RSF that has undergone the treatment of degumming and LiBr dissolution has blue fluorescence under 405 nm excitation wavelength, which may be caused by some specific amino acid residues or some metal elements combined with RSF.

In the control experiment, we collected the $CaCO_3$ particles produced without RSF, and then soaked them in 1 wt% RSF solution for 12 h. The particles obtained in this way were washed by DIW three times and collected by centrifugation. After being dried in air, no fluorescence can be seen in the dark field (Figure 7a, 7b). This suggests that conventional calcite don't have fluorescence and RSF adhered to calcite can be removed by washing in DIW. Calcite produced under high component concentration has blue fluorescence after washing by DIW (Figure 7c, 7d). This fluorescence is not the photonic-crystal coloration due to the heterogeneous structure of $CaCO_3$, but should come from the synergistic reaction of RSF and $CaCO_3$. Thus it is reasonable to conclude that these calcite particles are mediated by RSF. Similarly, hemisphere aragonite also has fluorescence after washing, and the fluorescent groups seem more in the upper surface than the back side (Figure 7e, 7f). This suggest that $CaCO_3$ particles just form beneath the air/water interface, where the interficial self-assembly RSF film can adsorb on the crystal upper surface and result in more fluorescence.

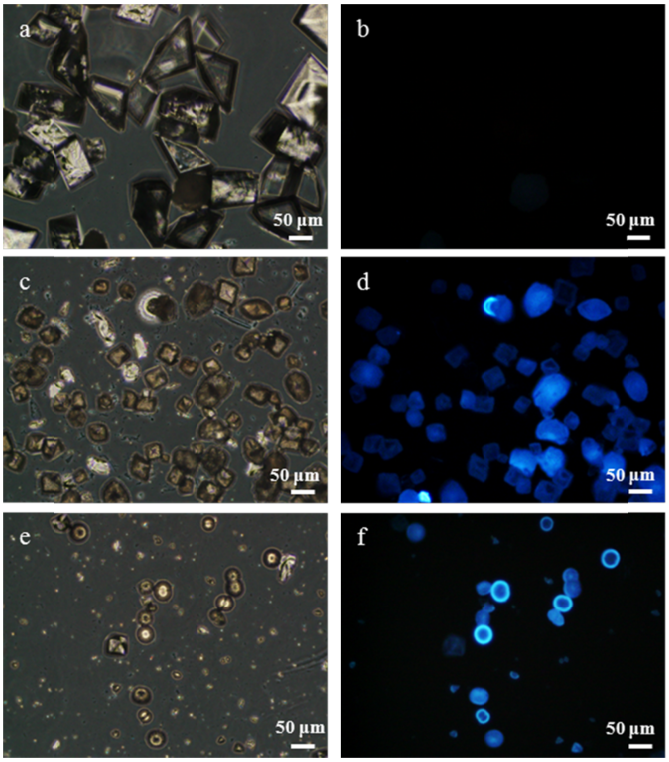

Figure 7 Confocal fluorescence microscope images of calcite particles obtained at the air/water interface after washing by DIW. Conditions: (a) and (b), [RSF] = 0, [Ca^{2+}] = 10 mM; (c) and (d), [RSF-83] = 1 wt%, [Ca^{2+}] = 10 mM; (e) and (f), [RSF-83] = 0.1 wt%, [Ca^{2+}] = 5 mM. (a), (c) and (e) are bright field images; (b), (d) and (f) are dark field images. Mineralization time: 72 h. The excitation wavelength: 405 nm. Blue: RSF.

Protein may have two effects on biomineralization, one is nucleation of the desired mineral phase, the other one is controlling the growth of the mineral.[21] Except the control experiment and those of extremely low concentrations of RSF, the mineralization in other conditions may experience a "nonclassical crystallization" process.[30] The initial stage of this process involves a liquid/liquid phase separation, which leads to an emulsified state of a highly hydrated liquid amorphous calcium carbonate (LACC).[22] In our system, a continuous "white liquid film" can be observed at 5 mM and 10 mM $CaCl_2$ solution under relatively high RSF concentration at 72 h

mineralization (Figure S4a, S4b), but was not found in the control experiment without RSF (Figure S4c, S4d). This emulsified-like film might be ascribed to LACC. Wolf *et al.* pointed out that acid proteins can stabilized LACC through a "depletion stabilization" and "de-emulsification" process.[22] In the presence of RSF, significant LACC may be stabilized for a month (or even longer) at the air/water interface in this experiment. When removed from solution, LACC shrinks to form solid amorphous calcium carbonate (SACC) in the form of the irregular material adhering on the crystals (Figure 6c) or nanowires connecting two particles (Figure 3i and Figure 6e), due to the rapid dehydration. SACC nanowires have blue fluorescence in confocal fluorescence microscope images (Figure S5), which might indicate RSF co-exit with ACC. Moreover, we can observe the hemisphere aragonite and flower-like calcite in high RSF and Ca^{2+} concentration. This radical growth process is commonly seen in polymer-induced ACC films, especially under high supersaturation.[23]

Crystals collected at the air/water interface are produced directly from ACC, with no vaterite phase observed in the mineralization process, which is different from that in the bulk solution[15, 24]. This suggested that the polymorph could be determined at the very beginning of the mineralization process. The structure of RSF at the air/water interface may play important roles in the selection between calcite and aragonite.

Here we propose a formation procedure for the $CaCO_3$ particles at the air/water interface assisted by RSF (Scheme 1). RSF can be adsorbed at the air/water interface and exhibit specific structures that depend upon the bulk concentration.[13] Ellipsometry data indicated a Langmuir RSF film is 11.6 to 11.9 Å thickness.[25] Thus we speculated the RSF chains templating $CaCO_3$ are laid on the layer and sub-layer of the air/water interface. For diluted RSF solution (≤0.02 wt%), RSF molecules tend to pack laterally in the adsorbed layer and seek more energetically favorable conformations,[13] e.g., helical silk III or laminated silk II.[16, 25, 26] These RSF molecules may act as anchors to form compact multi-layers.[13] A more stretched conformation at the interface resulted in more interaction zones between RSF chains in the surface layer and sub-surface layer.[13] The lateral packing RSF chains in the sub-surface are easier to form β-sheet (or β-strand) structure through hydrogen-bonding. β-sheets possess an intrinsic preferential ability to induce the crystallization of the aragonite phase,[15] which may be adsorbed on the aragonite crystal (010) face and promote crystal growth along the [001] long axis, resulting bundle-like aragonite.

For the concentrated RSF solution (≥1 wt%), RSF chains may adopt a hairpin-like conformation due to the crowded surface, resulting in the reduced interaction zones between surface and sub-surface layer.[13] The more disordered and large compact aggregates at the air/water interface are loosely interconnected,[13] which may inhibit the formation of compact β-sheets structure. Thus, calcite crystals are preferred in high concentration RSF.

When the RSF concentration was between 0.02 wt% and 1 wt%, RSF chains were crowded at the air/water interface, and it is more difficult to form β-sheet structure than in the diluted RSF solution. Under these conditions, Ca^{2+} concentration can affect the conformation of RSF, thus decide the morphology and polymorph of $CaCO_3$. Higher Ca^{2+} concentration may partially inhibit the formation of β-sheet structure, probably by introducing strong electrostatic interaction between RSF chains.[27] Thus, more calcite can be obtained at high Ca^{2+} concentration. Coexisting aragonite crystals produced under high Ca^{2+} concentration are hemi-spherical shape, which can indicate the compact and isotropic structure of RSF at the crowed air/water interface.

The aragonite particles produced here have two morphologies (bundle-like and hemisphere-like), which both grow directly from ACC. Generally, lower concentrations of RSF and Ca^{2+} result in bundle-like aragonite (Morph I). A main process of evolving from ACC is schematically illustrated in Scheme 1. The aragonite was assembled by much smaller nanoplates at the initial stage. With longer reaction times, the nanoplates preferred to tilt at both ends and further aggregate to form a bundle-like structure. The size of fan-shape sectors depended upon the component concentration, where less ACC or RSF may result a smaller edges of structures.

Hemisphere aragonite (Morph II) can be produced at high component concentration. Larger amounts of ACC and RSF chains can be inserted into the branches of the crystals at the very initial stage, resulting a hemisphere or hemi-gourd aragonite[28]. With longer reaction times, crystal size becomes larger, and the radical growth leads to the formation of a well-defined hemisphere aragonite. Moreover, SACC can be observed after the product has been collected, in the form of irregular material or nanowires.

Besides the calcite produced at extremely low RSF concentration, all the particles obtained have a concave upper surface. This might be caused by the less-ordered arrangement of the aggregated macromolecules,[8] due to the high molecular weight and multi-block structure of RSF, or by the balance of gravity and pulling force coming from the surface tension of the solution.[29] Thus the indentation in the center of the upper surface might be the nucleating point of the crystals at the core of the fans, and the crystals obtained from high RSF concentration may have a deeper indentation due to the aggregation of RSF and the low surface tension of the solution.

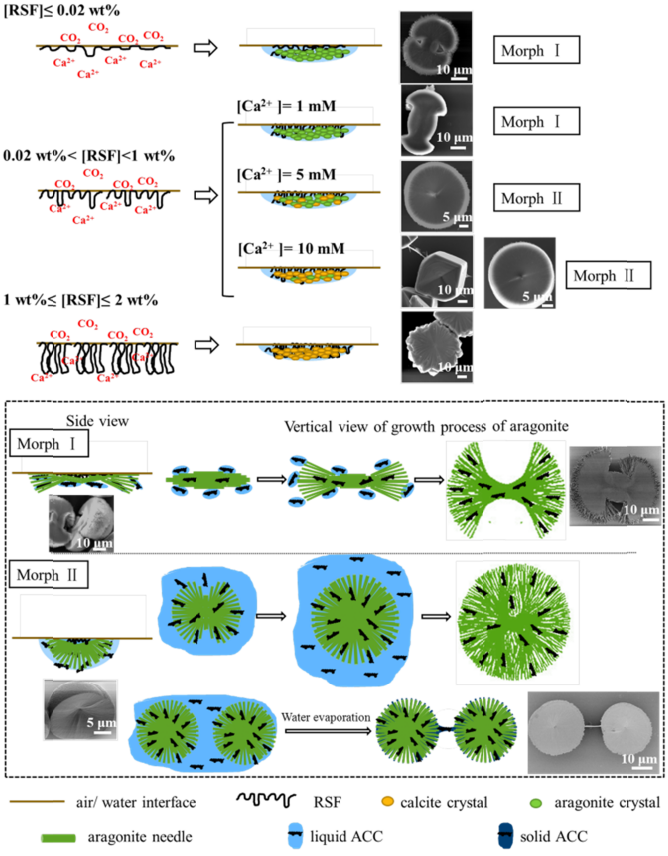

Scheme 1 Morphology and polymorph evolution process of $CaCO_3$ particles at the air/water interface mediated by silk fibroin. See text for details.

Our lab has found that molecular weight (MW) can influence the behavior of silk protein at the air/water interface, which is reflected in the surface tension results. High MW has higher surface activity

but lower adsorption efficiency. After mineralization under the same procedure, the morphology and polymorph of $CaCO_3$ particles vary with the MW of RSF. The morphology of $CaCO_3$ particles mediated by higher MW RSF (RSF-185) is shown in Figure S6, and the crystal polymorphs are summarized in Table 3. The mineralization results are similar to those mediated by RSF-83 at higher concentrations of RSF, while at lower concentrations, typical rhombus calcite is the dominant crystal instead of the aragonite mediated by RSF-83. This phenomenon can be ascribed to lower adsorption of high MW RSF. Moreover, aragonite particles mediated by RSF-185 are more "plump" and bigger than those mediated by RSF-83, due to the entanglement of high MW RSF. In contrary, aragonite mediated by low MW RSF (RSF-36) is smaller and thinner in morphology, with no hemisphere aragonite, and is found in greater quantities under higher RSF concentration (Figure S7). This should be due to the lower adsorption and lower entanglement of RSF-36. The polymorphs of the particles are similar to those mediated by RSF-83 (Table 3).

Table 3 $CaCO_3$ polymorphs obtained at the air/water interface with different concentrations of RSF-185 and Ca^{2+}

RSF / Ca^{2+}	2 wt%	1 wt%	0.2 wt%	0.02 wt%	0.002 wt%	0.0002 wt%	0.0001 wt%
1 mM	A+C	A	A	A	C+A	***C***	***C***
5 mM	C+***A***	C+***A***	***A***+C	A	C+A	***C***	***C***
10 mM	C	C	C+***A***	A+C	***C***	***C***	***C***

Note: The same meaning for capitals A and C as those in Table 2.

Table 4 $CaCO_3$ polymorphs obtained at the air/water interface with different concentrations of RSF-36 and Ca^{2+}

RSF / Ca^{2+}	1 wt%	0.2 wt%	0.1 wt%	0.02 wt%	0.002 wt%	0.0002 wt%	0.00002 wt%
1 mM	A/C	A	A	A	A	A	A+***C***
5 mM	C	A	A	A	A	A+***C***	A+***C***
10 mM	C	C	A	A	A	A+***C***	A+***C***

Note: The same meaning for capitals A and C as those in Table 2.

Conclusion

A series of $CaCO_3$ structures with a continuous variety in morphology and polymorphs were obtained at the air/water interface through the mineralization mediated by regenerated silk fibroins. The crystals can be formed from ACC directly with the aid of protein stabilization. Higher concentrations of RSF and Ca^{2+} resulted in calcite, while low concentrations induced aragonite. The morphology became plumper when increasing component concentration or RSF molecular weight. It was demonstrated that β-sheets formed at low concentration can absorb onto the crystal upper-surface and result in the aragonite phase, while the amorphous structure preferred at high concentration only produces calcite. Therefore, the selection of the final polymorph and morphology showed apparent dependence on the component concentrations and molecular weight of the RSF, but indeed the conformation of the protein at the air/water interface was critical for the mineralization results. This work demonstrated the control of RSF over the mineralization of $CaCO_3$ at the air/water interface, which provides a new way to understand the structure of RSF adsorbed at the interface. Moreover, the mineralization mediated by amphiphilic protein at the interface may become a new approach for producing materials with metastable polymorphs and complex morphologies.

Acknowledgements

This work is supported by the National Natural Science Foundation of China (No. 21034003) and Program of Shanghai Subject Chief Scientist (12XD1401000).

Notes and references

[a] State Key Laboratory of Molecular Engineering of Polymers, Advanced Materials Laboratory, Department of Macromolecular Science, Fudan University, Shanghai, 200433, People's Republic of China. E-mail: zzshao@fudan.edu.cn

[b] Department of Zoology, University of Oxford, South Parks Road, Oxford OX1 3PS, UK.

† Electronic Supplementary Information (ESI) available: [Surface tension of RSF solution, control experiment, Raman results, images of film-like layers formed at the air/solution interface and SEM images of calcium carbonate crystals mediated by RSF-185 and RSF-36 are included]. See DOI: 10.1039/c000000x/

1. D. C. Bassett, M. D. McKee and J. E. Barralet, *Crystal Growth & Design*, 2011, **11**, 803-810.
2. A. Lopez-Marzo, J. Pons and A. Merkoci, *J. Mater. Chem.*, 2012, **22**, 15326-15335; A. Sarkar, A. K. Ghosh and S. Mahapatra, *J. Mater. Chem.*, 2012, **22**, 11113-11120; X. Guo, L. Liu, W. Wang, J. Zhang, Y. Wang and S. H. Yu, *Crystengcomm*, 2011, **13**, 2054-2061; F. Huang, S. Li, J. Song, L. Chen, X. Zhang, Y. Shen and A. Xie, *Crystengcomm*, 2012, **14**, 1277-1282.
3. N. Sommerdijk and G. de With, *Chem. Rev.*, 2008, **108**, 4499-4550.
4. L. Addadi, D. Joester, F. Nudelman and S. Weiner, *Chemistry-A European Journal*, 2006, **12**, 980-987; Y. Levi-Kalisman, G. Falini, L. Addadi and S. Weiner, *J. Struct. Biol.*, 2001, **135**, 8-17.
5. C. Li and L. Qi, *Adv. Mater.*, 2010, **22**, 1494-1497; J. Yang, Y. H. Liu, T. Wen, X. X. Wei, Z. Y. Li, Y. L. Cai, Y. L. Su and D. J. Wang, *Crystal Growth & Design*, 2012, **12**, 29-32; H. Cölfen, *Angewandte Chemie International Edition*, 2008, **47**, 2351-2353; T. Sakamoto, A. Oichi, Y. Oaki, T. Nishimura, A. Sugawara and T. Kato, *Crystal Growth and Design*, 2008, **9**, 622-625.
6. J. C. Love, L. A. Estroff, J. K. Kriebel, R. G. Nuzzo and G. M. Whitesides, *Chem. Rev.*, 2005, **105**, 1103-1170; C. Lu, L. Qi, J. Ma, H. Cheng, M. Zhang and W. Cao, *Langmuir*, 2004, **20**, 7378-7380; E. M. Pouget, P. H. Bomans, J. A. Goos, P. M. Frederik and N. A. Sommerdijk, *Science*, 2009, **323**, 1455-1458.
7. X. X. Wei, Y. L. Su, T. Wen, Z. Y. Li, J. Yang and D. J. Wang, *Crystengcomm*, 2013, **15**, 3417-3422.
8. H. Cao, G. Q. Lin, J. R. Yao and Z. Z. Shao, *Macromolecular Bioscience*, 2013, **13**, 650-659.
9. S. Lee, J. H. Park, D. Kwak and K. Cho, *Crystal Growth & Design*, 2010, **10**, 851-855.
10. E. DiMasi, S. Y. Kwak, B. P. Pichon and N. A. Sommerdijk, *Crystengcomm*, 2007, **9**, 1192-1204; E. DiMasi, M. J. Olszta, V. M. Patel and L. B. Gower, *Crystengcomm*, 2003, **5**, 346-350.
11. E. Loste, E. Diaz-Marti, A. Zarbakhsh and F. C. Meldrum, *Langmuir*, 2003, **19**, 2830-2837.
12. R. Miller, V. Fainerman, A. Makievski, J. Krägel, D. Grigoriev, V. Kazakov and O. Sinyachenko, *Adv. Colloid Interface Sci.*, 2000, **86**,

39-82; J. Wiesbauer, R. Prassl and B. Nidetzky, *Langmuir*, 2013, **29**, 15240-15250.
13. Y. Yang, C. Dicko, C. D. Bain, Z. Gong, R. M. Jacobs, Z. Shao, A. E. Terry and F. Vollrath, *Soft Matter*, 2012, **8**, 9705-9712.
14. C. Cheng, Z. Shao and F. Vollrath, *Adv. Funct. Mater.*, 2008, **18**, 2172-2179; S. Sudo, T. Fujikawa, T. Nagakura, T. Ohkubo, K. Sakaguchi, M. Tanaka, K. Nakashima and T. Takahashi, *Nature*, 1997, **387**, 563-564.
15. T. Wang, D. Porter and Z. Shao, *Adv. Funct. Mater.*, 2012, **22**, 435-441.
16. R. Valluzzi, S. P. Gido, W. Muller and D. L. Kaplan, *International Journal of Biological Macromolecules*, 1999, **24**, 237-242.
17. R. Valluzzi, S. P. Gido, W. P. Zhang, W. S. Muller and D. L. Kaplan, *Macromolecules*, 1996, **29**, 8606-8614.
18. Y. Yang, Z. Shao, X. Chen and P. Zhou, *Biomacromolecules*, 2004, **5**, 773-779.
19. Q. Wang, Q. Chen, Y. Yang and Z. Shao, *Biomacromolecules*, 2012, **14**, 285-289.
20. H. J. Jin and D. L. Kaplan, *Nature*, 2003, **424**, 1057-1061; E. Leclerc and M. Daoud, *Macromolecules*, 1997, **30**, 293-300.
21. H. A. Lowenstam and S. Weiner, *On biomineralization*, Oxford University Press, 1989.
22. S. E. Wolf, J. Leiterer, V. Pipich, R. Barrea, F. Emmerling and W. Tremel, *J. Am. Chem. Soc.*, 2011, **133**, 12642-12649.
23. L. B. Gower, *Chem. Rev.*, 2008, **108**, 4551-4627.
24. S. Xu and P. Wu, *Crystengcomm*, 2013, **15**, 5179-5188.
25. W. S. Muller, L. A. Samuelson, S. A. Fossey and D. L. Kaplan, *Langmuir*, 1993, **9**, 1857-1861.
26. R. Valluzzi and S. P. Gido, *Biopolymers*, 1997, **42**, 705-717.
27. P. Zhou, X. Xie, D. P. Knight, X. H. Zong, F. Deng and W. H. Yao, *Biochemistry*, 2004, **43**, 11302-11311.
28. S. Xu and P. Wu, *Crystengcomm*, 2014, **16**, 1311-1321.
29. J. Lahiri, G. Xu, D. M. Dabbs, N. Yao, I. A. Aksay and J. T. Groves, *J. Am. Chem. Soc.*, 1997, **119**, 5449-5450.

